Journal of Sol-Gel Science and Technology 35, 115–122, 2005

Characterization of Porous Nanocomposites Formed by Cobalt Ferrites Dispersed in Sol-Gel Silica Matrix

JULIANA B. SILVA
Comissão Nacional de Energia Nuclear-CDTN/CNEN; Departamento de Química, UFMG, Belo Horizonte, Brazil 31270-901

CRISTINA F. DINIZ, ANA P.P. VIANA AND NELCY D.S. MOHALLEM*
Departamento de Química, UFMG, Belo Horizonte, Brazil 31270-901
nelcy@ufmg.br
nelcydsm@terra.com.br

Received July 19, 2004; Accepted March 31, 2005

Abstract. Composites of cobalt ferrite particles dispersed in a silica matrix ($CoFe_2O_4/SiO_2$) were prepared by the sol-gel process using tetraethylorthosilicate (TEOS) as a precursor of silica and metallic nitrates as precursors of ferrite. Samples of SiO_2 and $CoFe_2O_4/SiO_2$ were prepared in monolithic shape, dried at 110°C, treated at various temperatures and their characteristics were compared. After the thermal treatment, the surface area of the silica matrix decreased, above 700°C it densified, and above 1100°C it crystallized. The same heat treatment in the composite led to the crystallization of $CoFe_2O_4$ particles in the SiO_2 matrix and the increase in particle size, with the consequent increase in magnetization. The presence of particles in the matrix reinforced its structure, avoiding large changes in surface area and porosity and in the structure of the matrix after high temperature thermal treatment.

Keywords: cobalt ferrite, nanocomposite, silica matrix, sol-gel process, porous materials

1. Introduction

Cobalt ferrite is a promising material for the production of permanent magnets, magnetic recording media, magnetic fluids, and catalysts. As a nanocrystalline material, the correlation between ferrite magnetic and catalytic properties and particle size variation has been extensively studied [1–6]. Due to the possibility of development of new materials with atypical properties, composite materials formed by metallic or oxide particles dispersed in ceramic or vitreous matrices have been synthesized. Various magnetic systems like Fe [7], Ni [8], Fe_2O_3 [9], $NiFe_2O_4$ [10], and $NiZnFe_2O_4$ [1] dispersed in a silica matrix with applications in areas such as catalysis and electronics have already been developed.

In recent years, sol-gel process [11] has been used to produce magnetic composites [12] by the incorporation of ferromagnetic materials into a ceramic matrix. This type of composite is formed by nanocrystalline particles dispersed in an inert matrix with a high surface/volume ratio and as a result with different properties from those of bulk materials.

Matrix texture and the interaction between magnetic nanoparticles and the host can be used to improve the magnetic and physical properties, which depend both on the particle size, concentration of ferrites in the matrix and the composite nanostructure [1].

A better knowledge of the composite texture can be obtained if pore shape, size, and distribution, and

*To whom all correspondence should be addressed.

surface area are determined. In this work we have studied the textural characteristics of silica xerogels and cobalt ferrites dispersed in silica matrix [13] submitted to thermal treatment at different temperatures by gaseous adsorption [14–16]. Textural and structural changes of the materials were correlated with their magnetic properties.

2. Experimental

SiO_2 xerogels were obtained from the mixture of tetraethylorthosilicate, TEOS (Merck), ethyl alcohol and water in a 1/3/10 molar ratio with nitric acid as a catalyst. $CoFe_2O_4/SiO_2$ was obtained by adding 30 wt% of cobalt ferrites to the matrix solution in the form of nitrates, $Co(NO_3)_2 \cdot 6H_2O$ and $Fe(NO_3)_3 \cdot 9H_2O$ (Carlo Erba). The nitrate salts used in this work were chosen because they decompose at relatively low temperatures. Both precursor solutions, with pH maintained in the range between 4.0 and 5.0, were stirred at room temperature for one hour for homogenization and left to rest for gelation, which happened due to the hydrolysis and polycondensation of the metallic alkoxide. The wet gels obtained were submitted to aging at 60°C for 24 hours, dried at 110°C for 12 hours, and thermally treated at 300, 500, 700, and 900°C for 2 hours in air atmosphere. The monoliths obtained were divided in small pieces for characterization.

Simultaneous thermogravimetric and differential thermal analysis (TG-DTA) measurements were performed on TA Instrument SDT 2960. Samples previously annealed at 110°C were heated from room temperature to 1400°C at 10°C min^{-1} under airflow.

All samples (powdered) were analyzed by X-ray diffractometry (Rigaku, Geigerflex 3034) with Cu K_α radiation, with 40 kV and 30 mA, time constant of 0.5 s, goniometer velocity of 8° 2θ/min and crystal graphite monochromator to identify the phases present. Crystallite size was determined by Scherrer equation [17] ($D = 0.9\lambda/\beta\cos\theta$, where D is the average crystallite diameter, λ is the radiation wavelength and θ the incidence angle). The value of β was determined from the experimental integral peak width using silicon as a inner standard and by applying silicon standard correction for instrumental broadening [17].

The composition and purity of the composites were evaluated by an electron microprobe (Jeol JXA, model 8900RL) with an energy dispersive spectrometer (EDS) of the Laboratory of Micro Analysis/UFMG, and by infrared spectroscopy (Perkin-Elmer, model 2838).

Real density measures were obtained with a helium picnometer (Quantachrome) and apparent density by mercury picnometry. Sample textural characteristics were determined through nitrogen gas adsorption (Autosorb—Quantachrome Nova 1200) at liquid nitrogen temperature. Nitrogen gas was used for 5 hours with a 22-point adsorption-desorption cycle. The samples dried at 110°C were outgassed at 100°C for 3 hours, and the others were outgassed for 3 hours at 200°C before each analysis. Experiments were made in triplicate. Specific surface area and porosity were obtained by the application of Brunauer-Emmett-Teller (BET) equation [15] and the BJH method [15].

Magnetization measurements of composite samples were made in a vibrating sample magnetometer at 300 K with a maximum applied magnetic field of 1.0 T, taking into consideration the amount of ferrite in each sample.

3. Results and Discussion

Monolithic porous matrices and composites without defects after drying remained whole after thermal treatments in the range of 300 to 1100°C. Sample shape was defined by template. The silica xerogels were optically transparent until at 800°C and opaque after this, and the $CoFe_2O_4/SiO_2$ composite color changed from green to brown over 300°C.

TGA curve obtained for the matrix (Fig. 1(a)) shows a weight loss of 13% in the range of 25–150°C due to water and solvent removal, which corresponds to a broad endothermic peak in the DTA curve. Above this temperature we can observe a weight loss of 7% due to the loss of structural water due to condensation. In the DTA curve we can observe an exothermic event at 520°C associated to the decomposition of organic compounds in the structure of the matrix, and another at 1100°C associated to the crystallization of the silica as crystobalite. The composite (Fig. 1(b)) lost 20% weight in the range of 50–250°C due to water and solvent removal and to nitrate decomposition. We can observe an exothermic event at 250°C due to the crystallization of ferrite and a broad endothermic event between 600 and 1400°C associated with the densification of the composite.

SiO_2 matrix treated up to 900°C exhibited an amorphous behavior with an increase in the intensity and a narrowing of the XRD diffraction band

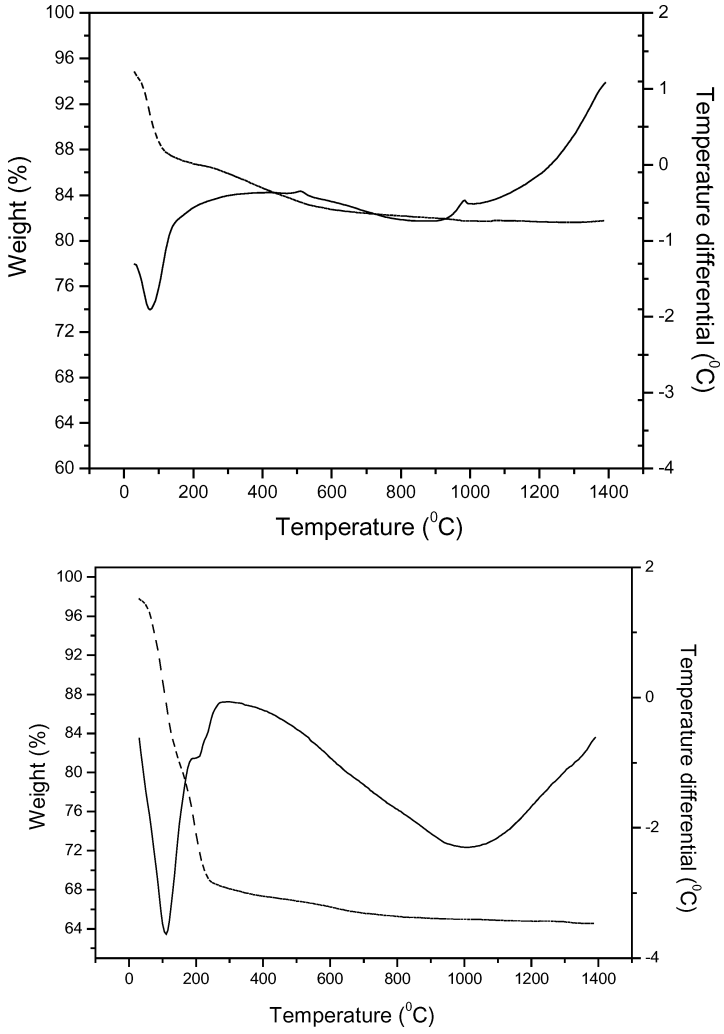

Figure 1. DTA/TG curves of (a) SiO_2 and (b) $CoFe_2O_4/SiO_2$.

with increasing temperature. This indicates an increase in the structural organization of the samples (Fig. 2). At 1100°C reflections characteristic of crystobalite and tridimite appeared. The composite exhibited an amorphous behavior up to 300°C. $CoFe_2O_4$ crystalline particles with cubic spinel structure were formed inside the amorphous silica matrix over this temperature (Fig. 3). During the formation of the $CoFe_2O_4$ nanocrystals, no traces of either crystobalite, or tridimite, or intermediate products were found even at temperatures as high as 1100°C, indicating that the ferrite particles were formed without binding to the matrix.

Figure 4 shows saturation magnetization (Fig. 4(a)) and crystallite size (Fig. 4(b)) changes with the increase in thermal treatment temperature. Ferrite average crystallite size was $< (10 \pm 1)$ nm when the sample was heated at 300°C and it increased with the calcination temperature (Fig. 4(b)). The samples only presented saturation magnetization over 400°C when the crystallites reached (10 ± 1) nm, which is in agreement with literature [2, 4]. We could observe that the saturation magnetization increased with the calcination temperature and stabilized above 700°C, and the crystallite size reached (40 ± 4) nm. The saturation magnetization of the composites whose ferrites had particle size of ∼90 nm was ∼20 emu·g^{-1}. Considering only the ferrite mass, the saturation magnetization was ∼65 emu/g, which is 81% of the saturation magnetization of the Co ferrite bulk (80 emu/g).

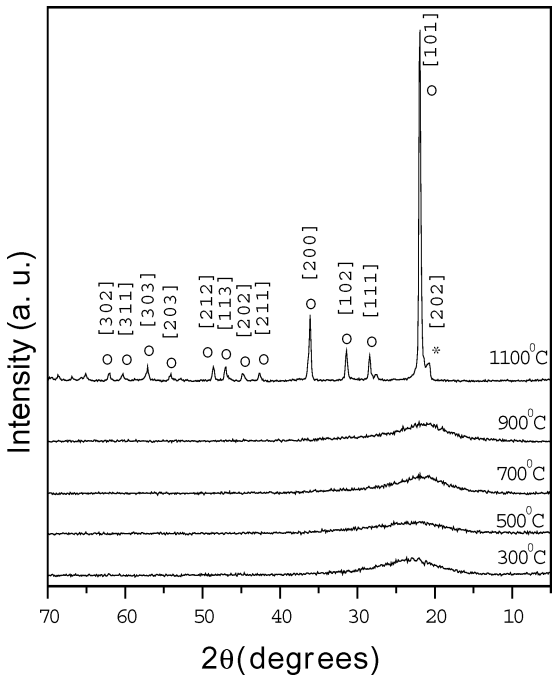

Figure 2. X-ray diffraction patterns of SiO_2 thermally treated in air for 2 hours at various temperatures. Crystobalite (○) and tridimite (∗).

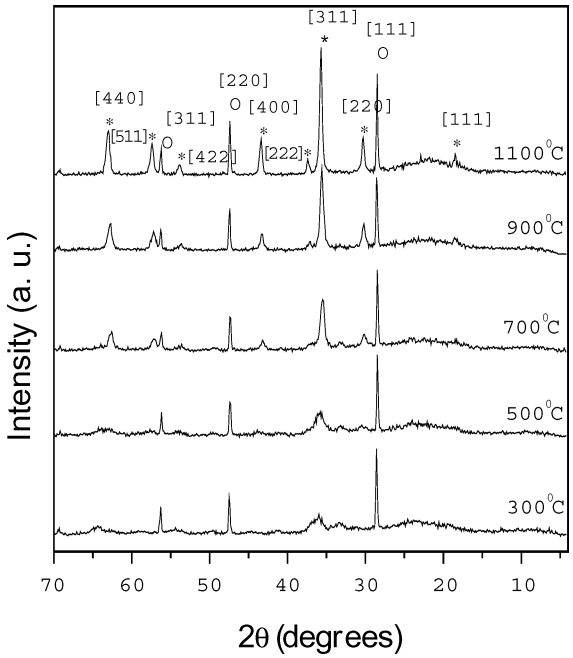

Figure 3. X-ray diffraction patterns of $CoFe_2O_4/SiO_2$ thermally treated in air for 2 hours at various temperatures. (○) silicon, (∗) $CoFe_2O_4$.

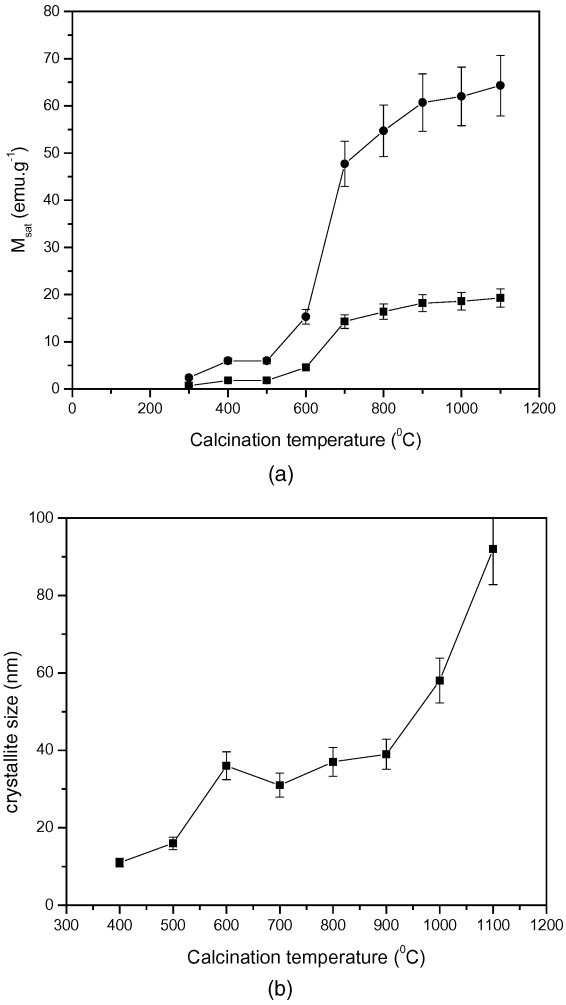

Figure 4. Variation of saturation magnetization, where (♦) shows M_{sat} for total mass and (▲) shows M_{sat} for ferrite mass (a) and particle size (b) with the calcination temperature of the composite 30 wt% $CoFe_2O_4/SiO_2$ prepared by sol-gel process.

Figure 5 shows the IR spectra of the composites obtained after heat-treating the dried gel at various temperatures for 2 hours. The IR spectra for the sample dried at 300°C had absorptions characteristic of the silica network at 1086, 810, and 461 cm^{-1}. The 1086 cm^{-1} band with the shoulder at 1160 cm^{-1} is due to the asymmetric stretching bonds Si—O—Si of the SiO_4 tetrahedron associated with the motion of oxygen in the Si—O—Si anti-symmetrical stretching. The 810 cm^{-1} band is associated with the Si—O—Si symmetric stretch and the band at 461 cm^{-1} with either Si—O—Si or O—Si—O bending. The 968 cm^{-1} band is composed of the contributions from Si—O—H and

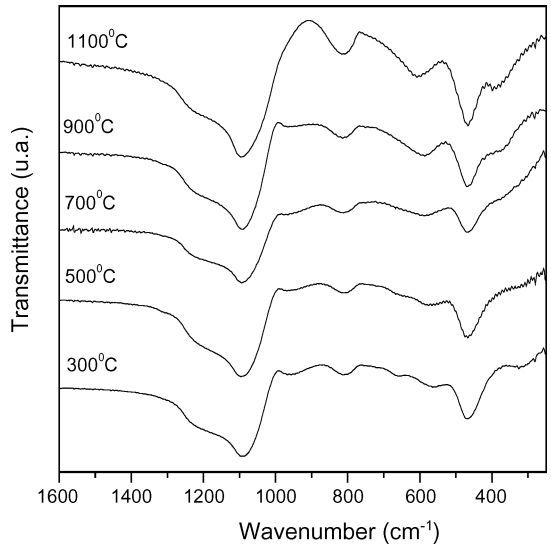

Figure 5. Infrared spectra of $CoFe_2O_4/SiO_2$ thermally treated in air for 2 hours at various temperatures.

Si—O—Fe vibrations, and the band at 584 cm^{-1} is related with the Fe—O stretching. The 968 cm^{-1} band disappears with the increase in temperature, showing that the weak bond between Si and Fe is broken. We can observe a slight shift of the 584 cm^{-1} band to the left. Co—O stretching vibration characteristic band appear also at 461 cm^{-1}. The weak band at 675 cm^{-1} can be due to the Co^{+} in tetrahedral centers in the matrix pores. These results are in agreement with those presented in literature [10].

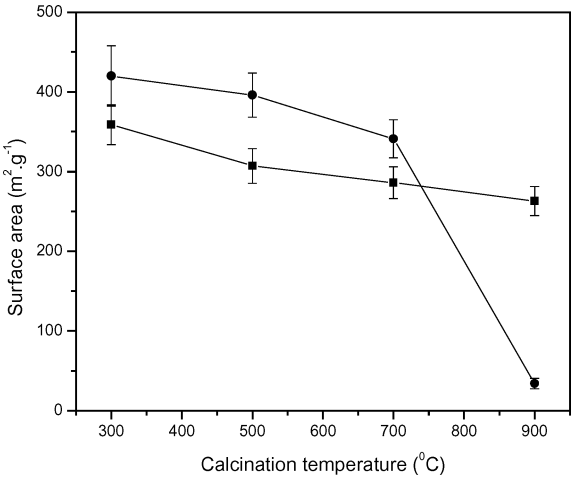

Figure 6. Variation of surface area as a function of temperature for composite de 30% $CoFe_2O_4$ in SiO_2 matrix (♦) and SiO_2 (●).

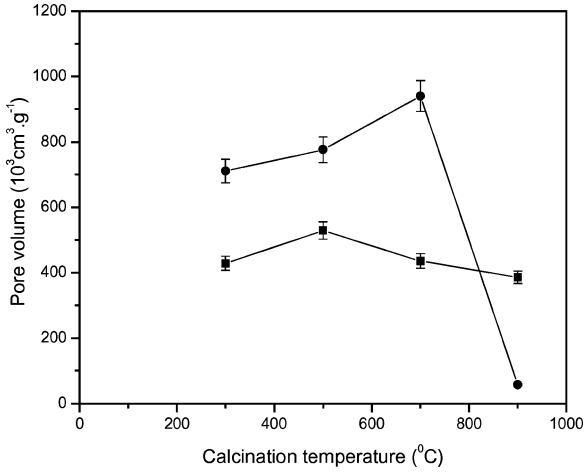

Figure 7. Variation of pore volume as a function of temperature for composite de 30% $CoFe_2O_4$ in SiO_2 matrix (♦) and SiO_2 (●).

Figure 6 shows the variation of surface area and Fig. 7 the total pore volume with the thermal treatment temperature of the silica xerogels and cobalt ferrite dispersed in the silica matrix. The textural characteristics of the silica xerogel changed substantially with thermal treatment (Table 1). Surface area and total pore volume decreased gradually over 300°C, and between 700 and 900°C there was a sharp decrease due to the collapse of the pores with the consequent shrinkage of the material structure. Composite surface area decreased gradually up to 900°C and the total pore volume stayed almost constant over all the temperature range because of the reinforcement of the silica structure due to the introduction of ferrite into the matrix [7]. Table 2 shows some textural parameters of the matrix and the composite at different temperatures. It has been observed that the composites have a smaller average pore radius than the matrix does. The C parameter or BET constant, which shows the degree of interaction between adsorbent and adsorbate had acceptable values, in the range of 40–210.

Table 1. Textural characteristics of SiO_2 xerogel as a function of heat treatment temperature (measurements are accurate to within ± 7%).

Treatment temperature (°C)	A_{BE} ($m^2 \cdot g^{-1}$)	Constante C	P_{BET} (%)	Average pore diameter (Å)
300	543	84	61	52
500	396	166	63	78
700	341	140	67	110
900	34	48	3	66

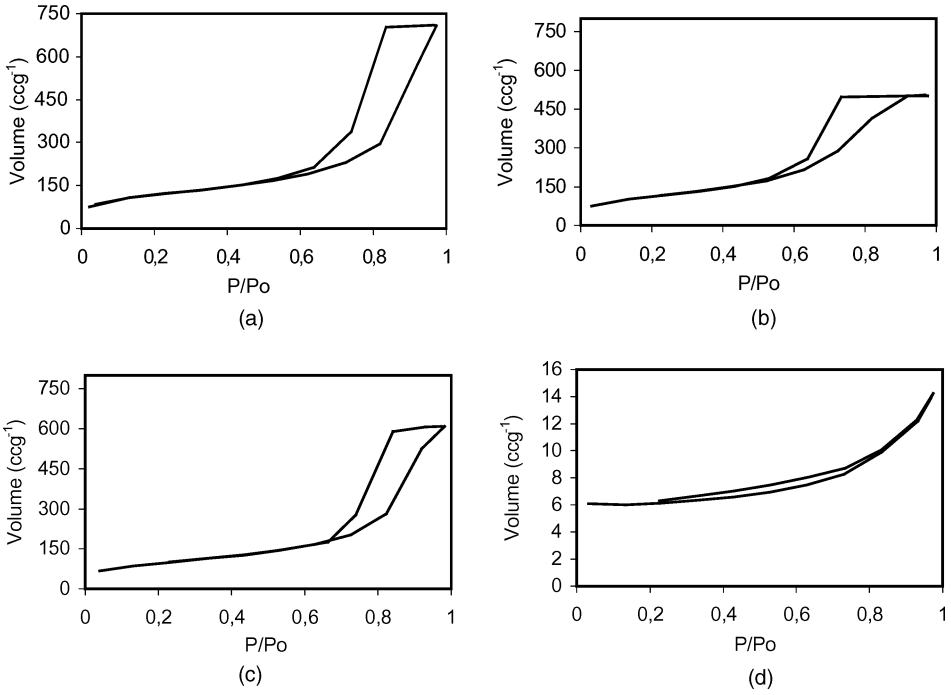

Figure 8. Adsorption/desorption isotherms of silica xerogel obtained for sol-gel method and heated at (a) 300°C, (b) 500°C, (c) 700°C and (d) 900°C.

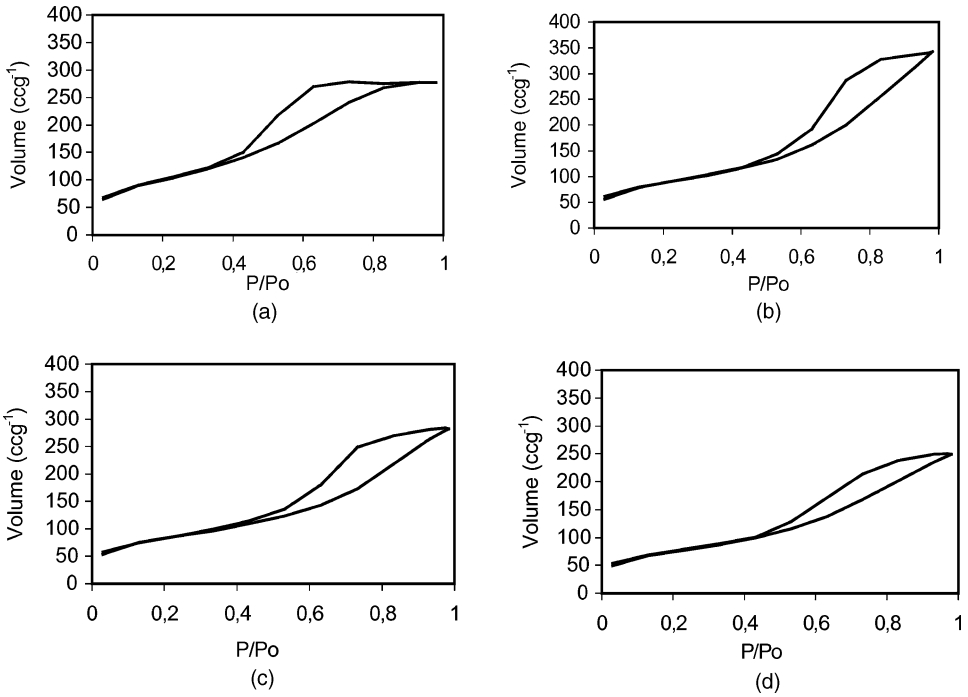

Figure 9. Adsorption/desorption isotherms of composite 30% de $CoFe_2O_4$ in SiO_2 matrix obtained for sol-gel method and heated at (a) 300°C, (b) 500°C, (c) 700°C and (d) 900°C.

Table 2. Textural characteristics of $CoFe_2O_4/SiO_2$ xerogel as a function of heat treatment temperature (measurements are accurate to within ± 7%).

Treatment temperature (°C)	A_{BET} ($m^2 \cdot g^{-1}$)	Constante (C)	ρ_r ($g \cdot cm^{-3}$)	ρ_{ap} ($g \cdot cm^{-3}$)	P_{BET} (%)	P (%)	Average pore diameter (Å)
110	221	84	1,86	2,35	52	25	60
300	359	128	2,16	1,09	57	65	48
500	307	208	2,21	1,19	62	62	68
700	286	258	2,31	1,21	58	61	60
900	263	178	2,45	1,61	55	48	58

ρ_e: real density, ρ_{ap}: apparent density, P_{BET}: porosity related to meso and micropores, P: total porosity.

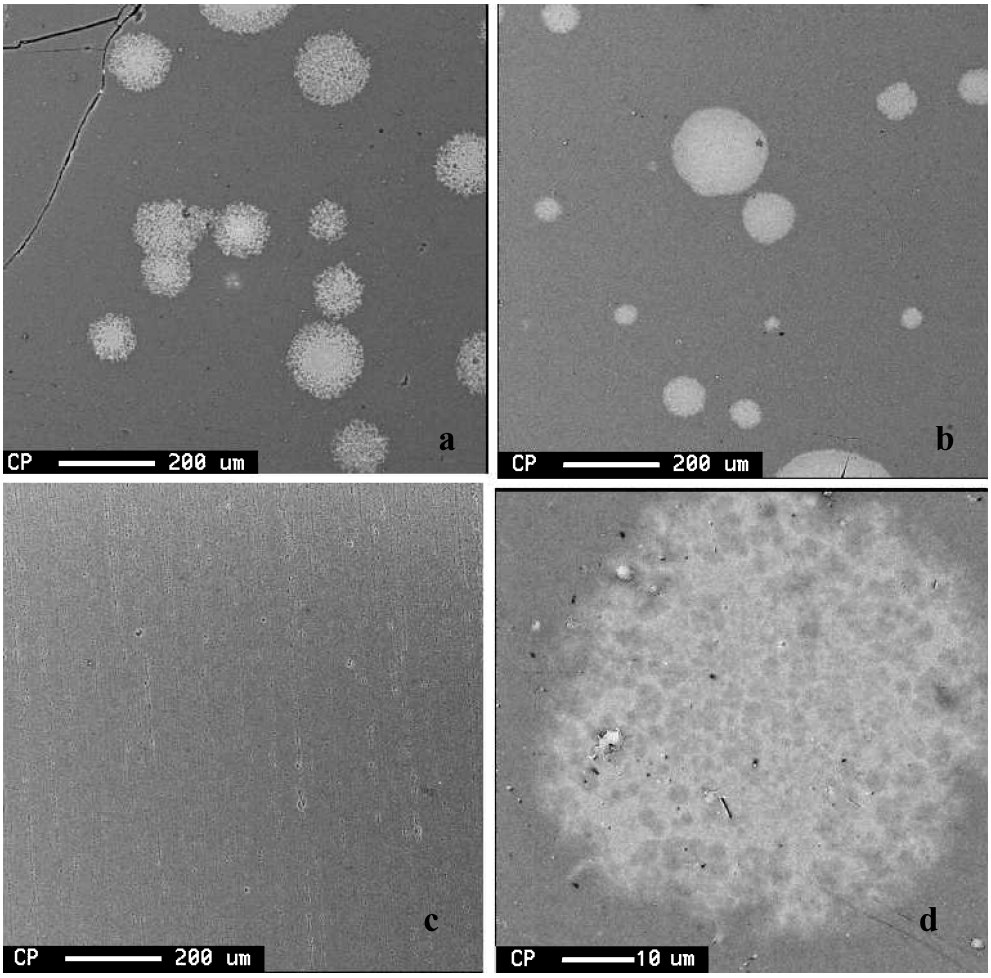

Figure 10. SEM images (backscattered electrons) of 30% $CoFe_2O_4/SiO_2$ composites treated at: (a) 300°C, (b) 700°C, (c) 1100°C and (d) white region.

Figures 8 and 9 show the adsorption-desorption isotherms for the matrices and the composites at different thermal treatment temperatures. The matrices treated at 300, 500, and 700°C adsorbed 700, 500 and 600 $cm^3 \cdot g^{-1}$ of gas, respectively, and presented type IV isotherm by BDDT [15] classification, characteristic of mesoporous materials with bottleneck pores. At 900°C, the amount of adsorbed gas decrease to

15 $cm^3 \cdot g^{-1}$ and the matrix showed a characteristic of a non-porous material (type III isotherm by BDDT classification). The composite (Fig. 9) have mesoporous characteristic at all preparation temperatures (type IV isotherm by BDDT [15] classification) with cylindrical pores open at both ends, and therefore with a minor difficulty of desorption. This fact is verified by the small variation in adsorption and desorption pressure for the same amount of adsorbed gas. The composites calcined at 300, 500, and 700°C adsorbed 280, 350, and 280 $cm^3 \cdot g^{-1}$, respectively, which was less than the amounts adsorbed by the matrices. However, the gas adsorbed by the composite calcined at 900°C was 250 $cm^3 \cdot g^{-1}$, an amount larger than the one adsorbed by the matrix calcined at the same temperature.

The backscattered electron image of the composite treated at 300°C (Fig. 10) shows distributed defined regions (white regions) in all the samples mostly as cobalt in the form of clusters as detected by EDS analyses. In the dark region, Si, Fe, O and traces of Co were detected. This result corroborates XRD and infrared ones, showing that initially iron was weakly bound to silica. As the calcination temperature increased, the clusters disappeared, and the cobalt diffused into the composite and bound to iron to form the ferrite. At temperatures above 900°C, EDS analyses detected a homogeneous distribution of Co and Fe in the composite, which is in accordance with IR and XRD results.

4. Conclusion

The formation and crystallization of $CoFe_2O_4$ into a SiO_2 sol-gel matrix reinforced its structure, producing a composite with specific surface area larger than that of the pure matrix at 900°C. We can speculate that the ferrite particles precipitated onto the pore walls, reinforcing the xerogel structure and at the same time filling part of them. The precipitate occurs in the form of clusters containing mostly cobalt, which diffused with the increase in temperature, binding to the iron that was initially bound to the silicon of matrix. At temperatures above 700°C, ferrite particles were formed inside the matrix pores. As a result, the surface area, total pore volume, and pore size of the matrix were larger than those of the composite, but less stable to temperature variation.

The composites presented a saturation magnetization that became more intense as crystallite size increased.

Acknowledgments

The authors thank the Brazilian agency FAPEMIG and CNPq for the financial support.

References

1. A. Chatterjee, S.K. Pradhan, D. Das, and D. Chakravorty, J. Magn. Magn. Mater. **127**, 214 (1993).
2. M. Grigorova et al., J. Magn. Magn. Mater. **183**, 163 (1998).
3. V. Masheva et al., J. Magn. Magn. Mater. **196/197**, 128 (1999).
4. C.L. Chien, Ann. Rev. Mater. Sci. **25**, 129 (1995).
5. A.S. Waniewska, P Didukh, J.M. Greneche, and P.C. Fannin, J. Magn. Magn. Mater. **215/216**, 227 (2000).
6. R. Shull, R.D. Ritter, and L.J. Swartzendruber, Appl. Phys. **67**, 4490 (1990).
7. C. Julián, G.A.P. Alcázar, F. Cebollada, M.I. Montero, J.M. Gonzalez, and J.F. Marco, J. Magn. Magn. Mater. **203**, 175 (1999).
8. G. Ennas, A. Mei, A. Musinu, G. Piccaluga, G. Pinna, and S. Solinas, J Non-Crystal. Sol. **232–234**, 587 (1998).
9. A. Corrias, G. Ennas, G. Mountjoy, and G. Paschina, Phys. Chem. Chem. Phys. **2**(5) (2000) 1045.
10. L. Guang-She, L. Li-Ping, R.L. Smith Jr, and H. Inomata, J. Molec. Struct. **560**, (2001) 87.
11. C.J. Brinker and G.W. Scherer, *Sol-Gel Science: The Physics and Chemistry of Sol-Gel Processing* (Academic Press Inc., 1990).
12. C. Estournès, T. Lutz, J. Happich, T. Quaranta, P. Wissler, and J.L. Guille, J. Magn. Magn. Mater. **173**, 83 (1997).
13. J.B. Silva, W. Brito, and N.D.S. Mohallem, Mater. Sci. and Engin. B **112**, 182 (2004).
14. L.Z. Wang, J. Yu, J.L. Shi, and D.S. Yan, J. Mat. Sci. Lett. **18**, 1171 (1999).
15. S.J. Gregg and K.S.W. Sing, in *Adsorption, Surface Area, and Porosity* (Academic Press Inc., New York, 1997).
16. S. Lowell and J.E. Shields, in *Power Surface Area and Porosity*, 2nd ed. (John Wiley, NY, 1992).
17. B.D. Cullity, in Elements of X-Ray Diffraction, A. W. P. C., 1987.